Decoupling microporosity and nitrogen content to optimise CO_2 adsorption in melamine-resorcinol-formaldehyde xerogels

Ivan A. Principe, Billy Murdoch, James M. Flannigan and Ashleigh J. Fletcher

Department of Chemical and Process Engineering, University of Strathclyde, Glasgow G1 1XJ, UK.

Highlights

- Concentration of basic functionalities increases as melamine content is increased
- Increased melamine lowers fixed carbon, raises volatile matter and weakens structure
- CO_2 adsorption capacity increases at 0°C and 60°C for higher melamine concentrations
- Melamine enhances CO_2 adsorption with a low enthalpy of regeneration
- CO_2 adsorption/desorption cycling measurements study show high sorption stability

Abstract

Selected melamine-resorcinol-formaldehyde (MRF) xerogels have been synthesised and analysed to determine the influence of nitrogen (N) incorporated into the gel structure, as well as, resorcinol to catalyst (sodium carbonate) and resorcinol to formaldehyde molar ratios. The aforementioned factors were varied, and their effect on gel properties characterised, allowing a better understanding of how gel characteristics can be tailored, and their impact on gel performance. MRF gels, produced in this study, were characterised using volumetric and gravimetric analyses to determine porous structure and quantify CO_2 capture capacities and kinetics, as well as allowing determination of heats of adsorption and activation energies for CO_2. MRF10_200_0.25 has exhibited the largest CO_2 capacity (1.8mmol/g at 0 °C) of the sample tested. Thermal stability was tested by proximate analysis, and MRF xerogels exhibited high thermal stability, however it was found that volatile matter increases as [M] increases, particularly for [M] 20%w/w and higher. Working capacity was determined from a series of cycling studies and capacities of 0.55, 0.58 and 0.56 mmol/g at 60 °C were observed for [M] of 10, 20 and 30%w/w, respectively. The measured heat of adsorption showed that incorporation of nitrogen functionalities results in a low energy penalty demonstrating that the adsorption mechanism is still driven by physical forces. The results obtained indicate that the family of materials studied here offer potential routes for carbon capture materials, through a combination of micropore structure development and incorporation of favourable Lewis acid-base interactions.

Keywords

FTIR; surface area; pore volume; pore size; gelation; Boehm titration; gravimetry.

Introduction

Carbon dioxide (CO_2) is currently considered to be the most important greenhouse gas (GHG), with a major impact on the global climate [1]. The GHG effect results from the accumulation of key gases in the atmosphere, which increase the temperature of the Earth, by trapping heat, giving rise to a global warming effect. The concentration of GHGs has varied naturally, according to different geological stages, nevertheless, through increased anthropogenic activities; this effect has been accentuated in recent years, particularly by increasing concentrations of CO_2, CH_4 and nitrous oxides.

As a result, the atmospheric concentration of CO_2 has increased from 280 ppm in the pre-industrial era to 520 ppm today [2]. This increase in CO_2 concentration is thought to drive global climate change and, for this reason, it is of vital importance that appropriate action be taken to stabilise and reduce CO_2 emissions. Hence, significant effort has been invested in the development of new technologies to reduce the emission of CO_2 to the atmosphere.

In recent years, several technologies have been developed to capture or concentrate CO_2, such as membrane separations [3-6], hydrate-based separations [7-9], cryogenic distillations [6,10,11], absorption systems [6,12-16] and adsorption processes [6,15,17-22]. Absorption processes have been widely applied industrially, however, solid sorbents for adsorption systems offer improvements on these systems and are promising alternatives for CO_2 capture from flue gases. The main issues related to absorption processes arise as a consequence of the required regeneration of the solvents used, which is a highly energy intensive and technically complicated process, due to the large volumes of sorbent and water required. Additionally, amines undergo degradation, resulting in solvent loss and corrosion of equipment, as well as generation of volatile compounds [16], which can themselves be nocuous for the environment and harmful to human health.

Carbon materials can be formed from gels, and particularly, Formaldehyde-Resorcinol (RF) resins, which are a type of organic material that have attracted attention due to their potential application in many processes, such as catalysis, thermal insulation, carbon capture, filtration, energy storage and as precursor of electrically conducting carbon material. RF gels, generally, exhibit a high pore volume, low density, large surface area and an amorphous structure. These parameters can be controlled and tailored as a function of the synthesis procedure [23], this characteristic make RF gels very attractive for a number of applications. Gels exhibits solid-like behaviour which is a consequence of a continuous network which extends throughout the volume of a liquid (solvent). The network is formed by cluster or group of molecules which are linked and interconnected. There are different contributions to this links such as methylene bridges, ether bridges, hydrogen bonding or chain entanglements. Organic aerogels, xerogels and carbon based materials have received a significant attention due to their potential applicability to gas treatment (adsorption) processes. The tune-ability of gels to tailor the structural properties to match specific requirements on given applications is attributed to the sol-gel process by which this materials are produced.

Attractive acid-base properties of solid materials can be exploited for CO_2 capture, and such interactions have been widely studied for activated carbons [24], however, little previous work has been undertaken on alternative organic materials derived from resorcinol-formaldehyde resins [25]. The incorporation of melamine into such structures modifies the surface groups of the final solid material [25]; this modification becomes important in applications including carbon capture because, by the addition of basic groups (such as amines) on the surface, the Lewis acid-base interactions (between CO_2 and surface) can be enhanced and, therefore, CO_2 adsorption capacity can be increased. Consequently, it is interesting to assess and quantify the effect of the degree of surface functionalisation. Here, the chemical and textural properties of a suite of xerogels are reported, selected for their similar microporous structures, but with varying degrees of modification with a nitrogen rich precursor (melamine), these samples provide a comparison of the effects of nitrogen content on CO_2 uptake, providing a basis for further materials optimisation for carbon capture technologies. This study represents an in-depth analysis of surface modification of resorcinol-formaldehyde xerogel by the incorporation of melamine into the structure.

Experimental procedure

Materials and Synthesis. Resorcinol (ReagentPlus, 99%), aqueous formaldehyde solution (37wt % formaldehyde, stabilized with 10 – 15% methanol), sodium carbonate (anhydrous, ≥ 99.5%), melamine (99%) and acetone (ACS reagent, ≥99.5%) were all purchased from Sigma-Aldrich.

The required composition of the MRF synthetic solution was calculated using the molar ratios of resorcinol to formaldehyde (R/F) and resorcinol to catalyst (R/C); sodium carbonate was the catalyst used for all samples. The volume of the solution was kept constant at 30mL and the total solids content (i.e. resorcinol, melamine, formaldehyde and carbonate) was fixed at 20% w/v, which corresponds to a solids content of 6g.

For the chosen R/C and R/F ratios and melamine concentration [M], the required mass of melamine was placed in a sealable 500mL jar with 25mL of deionized water (Millipore Elix 5 system). The melamine solution was heated up to ~50°C and stirred magnetically until complete dissolution of all solids. Then, the required resorcinol and carbonate masses were added to the solution while it was continuously stirred until complete dissolution was achieved. The required volume of formaldehyde solution was added to the jar together with additional water to a final volume of 30 mL, the jar was sealed and stirred for 30 min. Once the stirring period was complete, the pH of the solution was recorded using a Hanna pH 20 meter, fitted with an H1-1110B pH electrode, then the jar was resealed and placed in a pre-heated oven at 85 ± 5°C, as frequently used in previous studies [26]. The solution was left to gel for 3 days. Water contained within the pores of the gel network, upon completion of the gelation and curing periods, was removed via solvent exchange using acetone. The cured gel and 60 mL of acetone were shaken for 3 days at room temperature. The wet gel, after solvent exchange, was placed in a vacuum oven at a temperature of 90 °C in order to remove all remaining solvent from the pores of the gel. Sample nomenclature takes the form of MRFX_Y_Z, where X is the weight percentage of melamine, Y is the R/C molar ratio and Z is the R/F molar ratio. For example a sample produced using 10% w/w of melamine, an R/C of 100 and an R/F of 0.5 would be labelled as MRF10_100_0.5.

Xerogel Characterization. A Micromeretics ASAP 2420 system was used to obtain surface area and porosity data by nitrogen adsorption/desorption equilibrium measurements at -196 °C using ~0.5 g of sample. The sample was first degassed, at 120 °C for 120 min, prior to nitrogen sorption. Surface areas were calculated by applying Brunauer-Emmett-Teller (BET) theory [27], combined with the Rouquerol correction for BET application to microporous materials [28]. Pore volume was calculated from the equilibrium measurement of nitrogen adsorbed at 1 bar. The pore size distribution and average pore size was obtained by application of the Barret-Joyner-Halenda (BJH) method [29]. The t-plot method [1] was used to calculate the micropore volume and micropore surface area of all samples. CHN analyses were performed using a Perkin Elmer 2400 Series II CHNS Analyser. Results were obtained weight percentages, and were measured as a function of thermal conductivity; sample sizes were ~1-2 mg of xerogel per run. All samples were analysed by X-ray photoelectron spectroscopy (XPS Thermo Scientific Theta Probe) and Fourier transform infrared spectroscopy (FTIR-ABB Instrument MB3000 series S FTIR spectrometer with internal reflection diamond element), where each spectrum was the average of 86 of scans with spectral resolution 4 cm^{-1}. Xerogel samples were fully ground, and degassed, prior to FTIR analysis using a pestle and mortar assembly to obtain a homogeneous particle size.

All samples were analysed for equilibrium CO_2 adsorption capacity at 1 bar using an Intelligent Gravimetric Analyser (IGA001, supplied by Hiden Isochema Ltd), which allowed isothermal and kinetic data to be obtained. Additionally, all samples were tested for cycling capacity, using an IGA003 system (Hiden Isochema Ltd). For all gravimetric measurements, samples were outgassed prior to analysis, at a temperature of 120 °C under ultra-high vacuum (10^{-6} mbar) to a stable mass. Cycles were performed at 60 °C from a minimum pressure of 50 mbar to a maximum pressure of 1000 mbar.

Surface basicity was evaluated using a titration procedure based on Boehm's method; in brief, a known mass of MRF sample (~0.5 g) was added to 25 mL of 0.1 M HCl and shaken for 3 days, followed by 1 h of N_2 bubbling to remove any dissolved CO_2 from the solution. Two 10 mL aliquots were taken from each sample before direct titration with 0.1 M NaOH. All titrations were performed at room temperature with endpoint determination by both methyl red for standard titration and a Hanna pH 20 meter, fitted with an H1-1110B pH electrode, connected to data logging software, where the titrating solution was supplied by a syringe pump set at a flow rate of 2 mL min^{-1}.

Moles of carbon surface functionalities were quantified using the data obtained from the direct titration method and the relationship:

$$n_{CSF} = [Sol] \cdot V_{Sol} - [Titrant] \cdot V_{Tritant} \cdot \frac{V_{Sol}}{V_{Aliquot}} \qquad \text{(Equation 1)}$$

Where n_{CSF} represents the moles of basic functionalities on the surface of the MRF material that reacted with the acid used in the solution; *[Sol]* and V_{Sol} are concentration and volume of the solution, which represent the moles of acid available in the solution to react with the surface groups of the MRF. *[Titrant] and* $V_{Titratnt}$ are the concentration and volume of titrant used, which represent the moles of titrant that react with the remaining moles of acid from the solution after reaction with the sample, and $V_{aliquot}$ is the volume of the aliquot taken from the solution for titration.

Thermal stability and proximate analyses were performed on all xerogel samples to understand the proportion of moisture, volatile matter, fixed carbon and ash in the material. This analyses was performed using a Netzsch STA 449 F3 Jupiter model. Thermal gravimetric analysis (TGA) was used to monitor the mass loss for xerogel samples as a function of temperature. Additionally, Differential Scanning Calorimetry (DSC) was used to determine the energy transitions (exothermic or endothermic) occurring as a function of temperature. The equipment is fitted with a highly sensitive balance and a silicon-carbide furnace (room temperature to ~1500 °C). Samples did not require special preparation for this test, and the mass of xerogel used ranged from 23 to 35 mg.

Density is defined as the ratio of mass to volume, therefore, a known mass of sample, weighed on an analytical balance, was placed in a 5 mL volumetric flask. Successively, the flask was filled to the maximum volume with a known volume of deionized water, produced in house (Millipore Elix 5 system). The system was agitated to remove any air from the sample before the container was topped up with additional water, as required. The volume displaced by the known mass of xerogel was subsequently used to determine the density.

Results and Discussion

Textural properties: The suite of MRF materials analysed in this study were synthesised by varying the proportion of the reactants (melamine, resorcinol, formaldehyde and sodium carbonate) in the synthetic matrix. Materials were selected from a wider family of 100 gels [25], produced with varying R/C and R/F, as well as [M], on the basis of their micropore volume (Table 1), aiming to provide a suite of samples with varying nitrogen contents but similar micropore volumes to allow direct comparison of any observed differences in CO_2 capacity in terms of [M]. MRF0_100_0.5, MRF1_400_0.5, MRF10_200_0.25, MRF20_100_0.25, MRF30_50_0.25 and MRF40_50_0.25 all exhibit micropore volumes of ~0.03 $cm^3\ g^{-1}$, allowing a comparison of their performance in terms of CO_2 adsorption uptake, and providing a basis to observe the effect of increasing nitrogen content on CO_2 adsorption capacity. Other samples were included in the study to observe the impact of increasing R/C for MRF0 and MRF1 samples. MRF0_50_0.25 exhibits a high density; combined with its narrow pore size, and the smallest pore volume of the samples selected, this suggests a highly compact structure for this particular sample. By contrast, MRF10_200_0.25 has an even greater density than MRF0_50_0.25, but its average pore size is 6 times larger and the total pore volume is almost double, therefore, the inherent surface area should be more accessible for adsorption and gas diffusion, suggesting differences in behaviour should be observed for these samples.

Table 1: Total (BET), non-micropore and micro surface area, total pore and micropore volume and pore size obtained for MRF xerogels synthesised in this study.

Sample	Surface Area (BET and t-plot)			Pore Volume		BJH		Elemental Analysis			Surface functionality
	Total (m^2/g)	non-micropore (m^2/g)	Micropore (m^2/g)	Total (cm^3/g)	Micropore (cm^3/g)	Pore Size (nm)	Density[†] (cm3/g)	Carbon (w/w %)	Hydrogen (w/w %)	Nitrogen (w/w %)	Ncsf µmol/g
MRF0_50_0.25	442	258	184	0.24	0.08	2	1.20(11)	61.7	5.1	0.0	-
MRF0_100_0.25	476	369	106	0.33	0.05	3	0.76(03)	57.0	5.2	0.0	-
MRF0_200_0.25	464	365	99	0.60	0.04	5	0.81(03)	59.9	4.8	0.0	-
MRF0_100_0.5	446	369	74	0.31	0.03	3	1.01(06)	62.7	4.7	0.0	-
MRF1_100_0.25	480	389	92	0.38	0.04	3	0.96(04)	57.5	5.3	0.8	0.22
MRF1_400_0.5	256	187	69	0.65	0.03	11	0.79(03)	61.7	4.9	0.8	0.36
MRF10_200_0.25	194	143	61	0.44	0.03	12	1.43(09)	57.1	5.0	8.8	0.71
MRF20_100_0.25	303	228	74	0.76	0.03	11	1.17(08)	53.1	4.9	16.0	0.85
MRF30_50_0.25	428	345	83	0.82	0.04	8	0.65(02)	50.2	4.8	22.2	1.64
MRF40_50_0.25	351	286	58	0.80	0.03	10	1.05(06)	47.8	4.8	29.4	2.49

[†] the value stated in parentheses indicates the uncertainty in the last two digits of the reported density.

The isotherms obtained from N_2 adsorption on the MRF xerogels studied here (Figure 1a-c) can be classified as Type IV [2], which indicates mesoporous solid sorbents. The pore filling mechanism involves initial monolayer coverage followed by multilayer adsorption and, finally, capillary condensation. The hysteresis loops are of two distinct shapes: H1 and H2. H2(a) is observed for low [M] (MRF0s and MRF1_100_0.25); while, MRF1_400_0.5 exhibits a shape closer to H2(b), and samples with higher [M] show a mix of behaviour between H2(b) and H1. The trend in moving from H2(a) to H2(b) and H1 seems to be a general one when increasing [M], but it is arguable that the shape of the hysteresis loops for MRF10, MRF20, MRF30 and MRF40 xerogels (Figure 1) corresponds to H2(b), H1 or a mix of both. Type H1 is, generally, attributed to porous materials, agglomerates or compacts with uniform spheres in a regular array, hence, narrow distributions of uniform mesopores. By contrast, the pore distribution and shapes are not well defined for Type H2, however, it is usually related to 'ink bottle' shaped (narrow neck and wide body) pores.

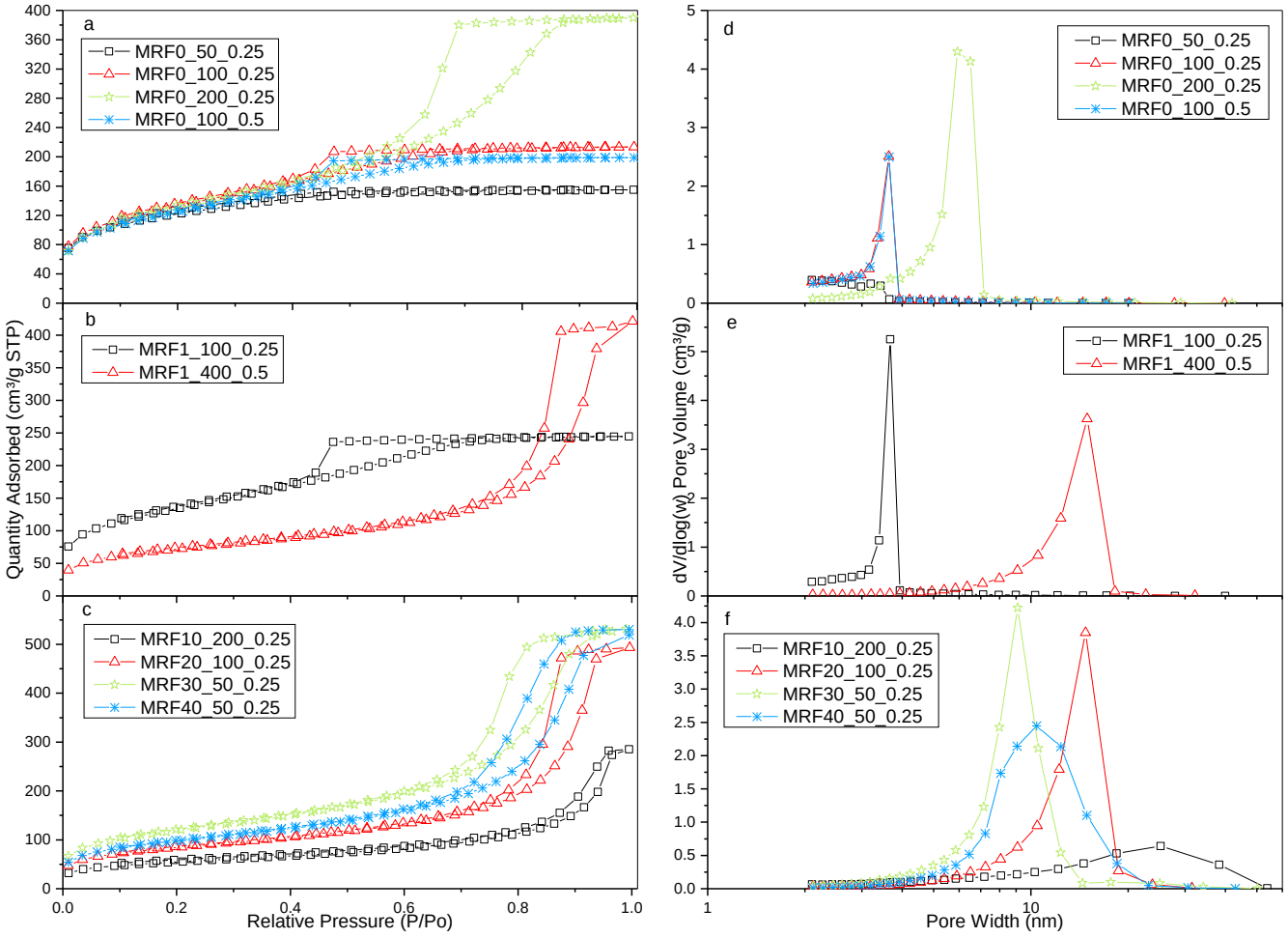

Figure 1: **(a) N_2 adsorption isotherms and (d) pore size distributions for MRF xerogels synthesised in this study using variable R/C and R/F for [M] 0 w/w%; (b) N_2 adsorption isotherms and (e) pore size distributions for MRF xerogels synthesised in this study using variable R/C and R/F for [M] 1 w/w%; (c) N_2 adsorption isotherms and (f) pore size distributions for MRF xerogels synthesised in this study using variable R/C and R/F for [M] 10, 20, 30 and 40 w/w%.**

The pore size distributions (Figure 1d-f) show an increase in average pore size as melamine content is increased [25]. It is worth mentioning that other variables (i.e. R/C and R/F) rather than melamine

content varies among the samples presented, however pore size follows the same trend (for increasing [M], as observed previously [25]. Figure 1d allows a comparison for increasing R/C with constant R/F and [M]. The samples, MRF0_50_0.25, MRF0_100_0.25 and MRF0_200_0.25, show an increase in pore size, from 2 to 5 nm with increasing R/C, which is consistent with reports in the literature for both RF and MF materials [30,31]. MRF0_100_0.5 exhibits an identical isotherm and pore size distribution as MRF0_100_0.25, suggesting that R/F has little effect at the levels studied. Results are consistent for MRF0_100_0.25 and MRF1_100_0.25 with the same R/C and R/F, and only a minor difference in [M]; therefore, these samples exhibit similar textural character. Average pore size increases as [M] is increased and there is an associated increase in N_2 uptake at low [M]. This increase in pore volume does not, however, necessarily translate to an increase in CO_2 uptake, given that not all volume available results in useful interactions with CO_2. MRF1_400_0.5 has a noticeably larger pore size than MRF1_100_0.25, which can be attributed to the higher R/C used. The degree of crosslinking of RF xerogels decreases as [M] increases, affecting the porous characteristics, as can be seen in Table 1, i.e. addition of melamine into the structure of MRF0_50_0.25 to MRF40_50_0.25, increases the average pore size and pore volume, while reducing the surface area and the proportion of microporosity. Thus, [M] has a significant impact on the structural properties of MRF xerogels and can be used to tailor desired characteristics.

Chemical analysis: Elemental analysis was used to quantify the compositional proportions of carbon, hydrogen and nitrogen (CHN), and to confirm the level of nitrogen incorporated into the final xerogel structure. Results are shown in Table 1, and it is evident that there is a direct correlation between nitrogen content determined and [M] used in the xerogel synthesis. Titration analysis provided information about the changes in surface chemistry upon introduction of melamine into the structure. Particularly, surface modification is attributed to the amine groups present in the structure of melamine, which represent basic moieties. Results obtained for MRF0s xerogels show a small degree of fluctuation around zero, which suggests that no basic functionalities are present in xerogels formed without melamine. The quantities of carbon basic surface functionalities (Ncsf) obtained for samples with [M] ≥ 1 were calculated using Equation 1 and the results obtained are shown in Table 1. Samples made with ≥ 1 w/w% of melamine show a clear increasing trend in the number of basic carbon functionalities with increasing melamine content. This confirms the incorporation of melamine into the structure and surface functionalisation by amine groups.

FTIR analysis (see Supporting Information Figure SI 1) showed three main acidic frequencies for these systems and the data suggest that, of these, no lactonic or carboxylic groups are present (absence of peaks at 1765 cm^{-1} and 1690 cm^{-1}, respectively), but does indicate phenolic structures from the O-H stretch at 3550-3200 cm^{-1} [32]. As [M] increases in the synthetic matrix, less resorcinol is used; hence, the final structures are expected to exhibit fewer phenolic groups in the final materials. The FTIR spectra obtained for all samples show a peak attributed to phenolic functionalities (3200-3500 cm^{-1}) [32], which changes with varying [M]. For MRF40_50_0.25, proportionality of the peaks in the fingerprint region compared to the O-H peak increases considerably, suggesting that the concentration of O-H groups is lower compared to the concentration of the skeletal bonds (observed in the fingerprint region). By comparison, the MRF0 xerogels exhibit O-H peak and fingerprint region intensities that are very similar, suggesting as many -OH bonds or groups as C-O or C-H structural groups. The peak observed at ~2350 cm^{-1} likely corresponds to surface adsorbed CO_2, which vibrates at 2349 cm^{-1} [32]. While the shoulder between 2950 and 2850 cm^{-1} can be ascribed to C-H stretching vibrations, supported by the peak observed at ~1490 cm^{-1}, which is related to C-H deformations. The

C=O bond gives a peak at 1640-1595 cm^{-1}, however, it could also be attributed to primary or secondary amide functionalities, which vibrate at ~1650 cm^{-1} and 1570-1515 cm^{-1}, respectively [32]; peak intensity, hence concentration of groups, increases as [M] in increased.

There is a peak at ~1300 cm^{-1}, the intensity of which seems to increase as [M] is increased; this peak is likely associated to the C-N stretching vibration (1360-1080 cm^{-1}) [32], for amine groups. Additionally, C-O has a strong interaction at 1300-1020 cm^{-1} [32], hence, the peak observed at ~1150 cm^{-1} is possibly associated with this vibration. Finally, there are strong peaks at 850-700 cm^{-1}, which can be ascribed to C-H peaks for aromatic groups.

The presence of C=O bonding was also observed by XPS (see Supporting Information Figure SI 3-6), and incorporation of nitrogen into the xerogel structure can be seen in Figure 2. The results confirm the increase of nitrogen content as [M] increases. XPS showed marginally different elemental analysis values compared with CHN, which can be ascribed to the sensitivity of XPS to the presence of contaminants. XPS also showed that C=O bonding increases with increasing [M] (see Supporting Information Figure SI 3-6), which is in agreement with results obtained by FTIR. The binding energies observed for these samples indicate pyridinic and amine functionalities[33] within these carbon rich materials, which is consistent with the moieties present in the precursor materials.

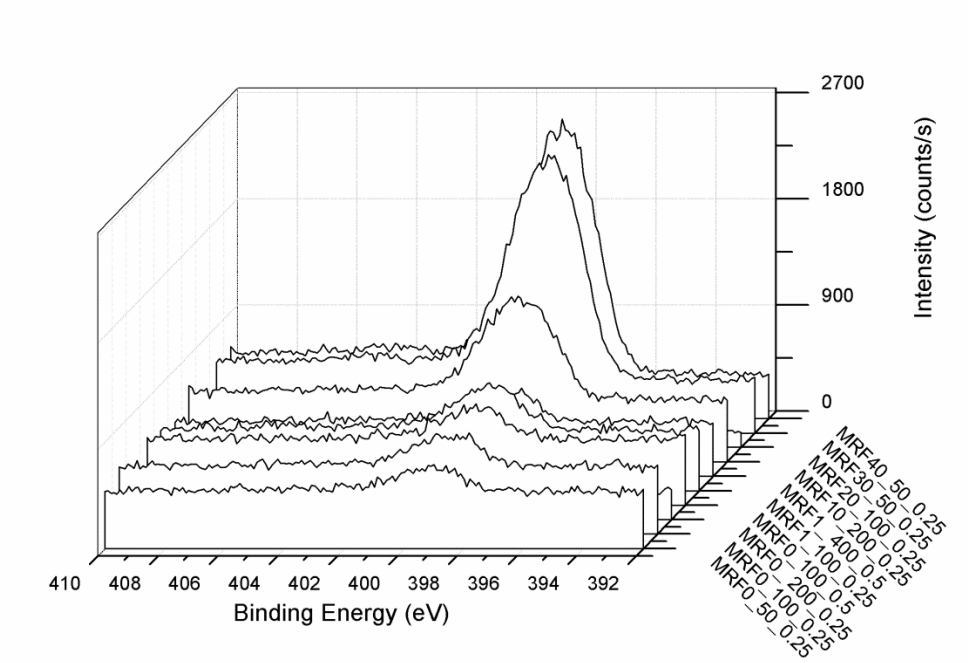

Figure 2: XPS measurement of nitrogen binding energy in MRF xerogel samples.

The increasing concentration of C=O bonding within the gels is ascribed to polymerisation reactions occurring during gelation (see Supporting Information Figure SI 3-6), as presented in Scheme 1. Resorcinol is more reactive that melamine, hence, formaldehyde addition to resorcinol is more favourable; therefore, even at higher [M], formaldehyde would likely be consumed first, producing a compound with no C=O bonding. By contrast, reaction of formaldehyde with melamine forms a compound, where conjugation cannot occur as a consequence of the stable 'R-N-C bonds within the structure, hence, C=O moieties would not be consumed in further reaction but would tend to be retained within the structure. This also explains the mechanical weaknesses observed for xerogels

with increased [M], as the degree of cross-linking is expected to decrease as [M] increases. However, Melamine substitutes part of the Resorcinol needed stoichiometrically, therefore, as [M] concentration increases more Formaldehyde will inevitably react with the Melamine present increasing the presence of C=O as observed in Figure 2.

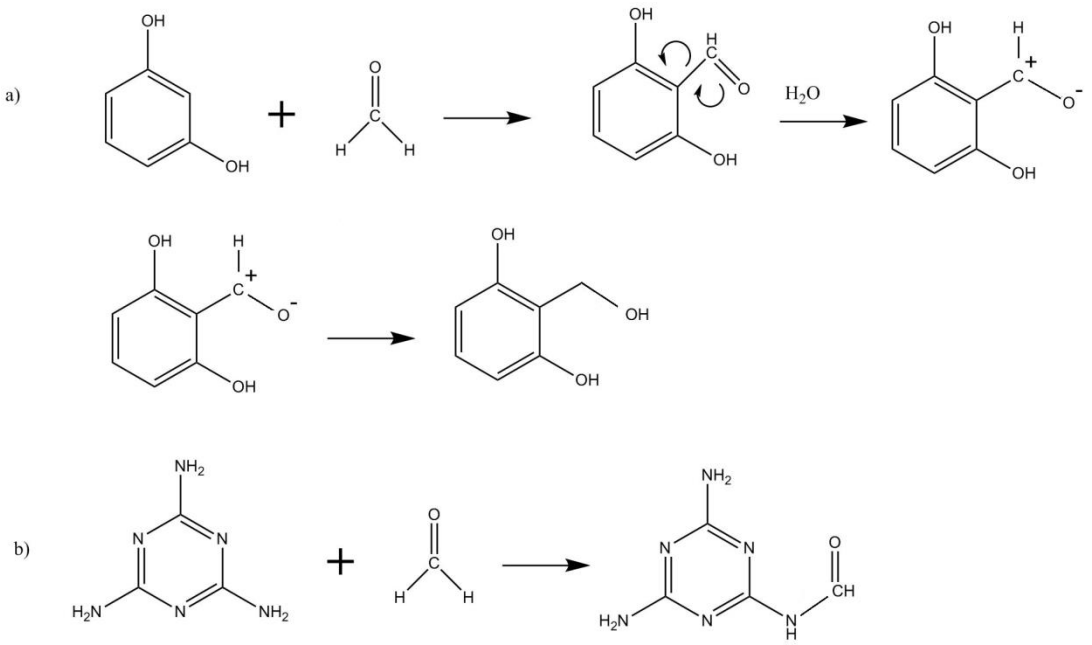

Scheme 1: Reaction of formaldehyde with (a) resorcinol and (b) melamine

Composition was determined by TG and DSC measurements. After the endothermic loss of moisture (~10%) at 120 °C, volatile matter is decomposed up to 920 °C, and the exothermic combustion of fixed carbon (820 °C in air) results in a final mass of the ash content (see Supporting Information Figure SI 7-9). Volatile losses occur at 200-750 °C, with multiple exothermic reactions occurring at different temperatures within this range. The intensity of the narrow peak at 345 °C increases markedly as [M] is increased; this peak corresponds to decomposition of the resin's structure, at the sublimation temperature of melamine (345 °C) [34]; correspondingly, fixed carbon content decreases as [M] increases. These results confirm the lower level of crosslinking for samples with higher melamine contents, as there is little chemical change to the melamine added, and the reduction of carbon in the structure as it is replaced by nitrogen present in melamine (triazine). Negligible mass remains after combustion of fixed carbon, as expected for organic based materials.

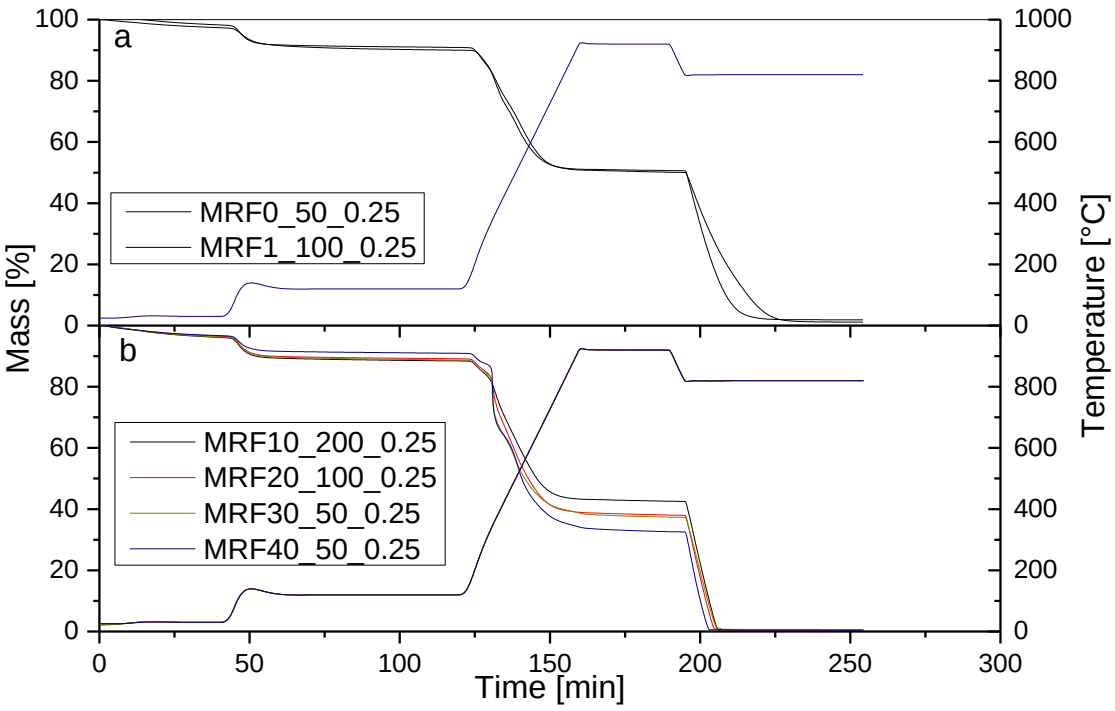

Figure 3: **Thermo-gravimetric (TG) analysis of MRF xerogels, mass loss (TG) and temperature programme used. The measurement was carried out in a N_2 atmosphere from room temperature to ~920 °C, then temperature is set to ~820 °C and air is used instead.**

Table 2: **Proximate analysis showing mass percentage composition in MRF xerogel samples analysed.**

Sample	Moisture	Volatile matter	Ash	Fixed carbon
MRF0_50_0.25	9.99	39.89	1.13	48.99
MRF0_100_0.25	13.39	37.72	0.76	48.13
MRF0_200_0.25	11.10	42.50	0.48	45.91
MRF0_100_0.5	10.62	40.07	1.13	48.17
MRF1_100_0.25	9.09	40.24	1.88	48.79
MRF1_400_0.5	10.14	43.13	0.88	45.84
MRF10_200_0.25	11.56	45.86	0.45	42.12
MRF20_100_0.25	10.86	51.08	0.40	37.66
MRF30_50_0.25	11.28	51.32	0.64	36.76
MRF40_50_0.25	9.08	58.30	0.40	32.22

CO_2 adsorption: CO_2 uptake capacities were tested at 0 and 60 °C (see supporting information Figure SI 10) and, as expected for physisorbed systems, the equilibrium uptake of CO_2 decreased with increasing temperature. An increase in CO_2 adsorption is observed, at each temperature, as [M] is increased, confirming the expected enhancement of adsorption capacity by incorporation of nitrogen into the structure, which increases adsorption by exploiting the Lewis acid-base interactions between CO_2 molecules (acidic character) and basic functionalised adsorption sites on the surface of the MRF xerogels.

CO_2 adsorption isotherms obtained (Figure 4) exhibit Type I character, as classified by IUPAC [2], indicative of microporous materials; given the predominantly mesoporous character of the MRF materials tested, it is likely that adsorption of CO_2 is limited, under the conditions used, to the microporous region. When isotherms are normalized with reference to the surface area of each

material (Table 1), a significant increase in CO_2 adsorption is seen at both at 0 and 60 °C, which is attributed to the effect of nitrogen incorporated into the structure of the MRF xerogel.

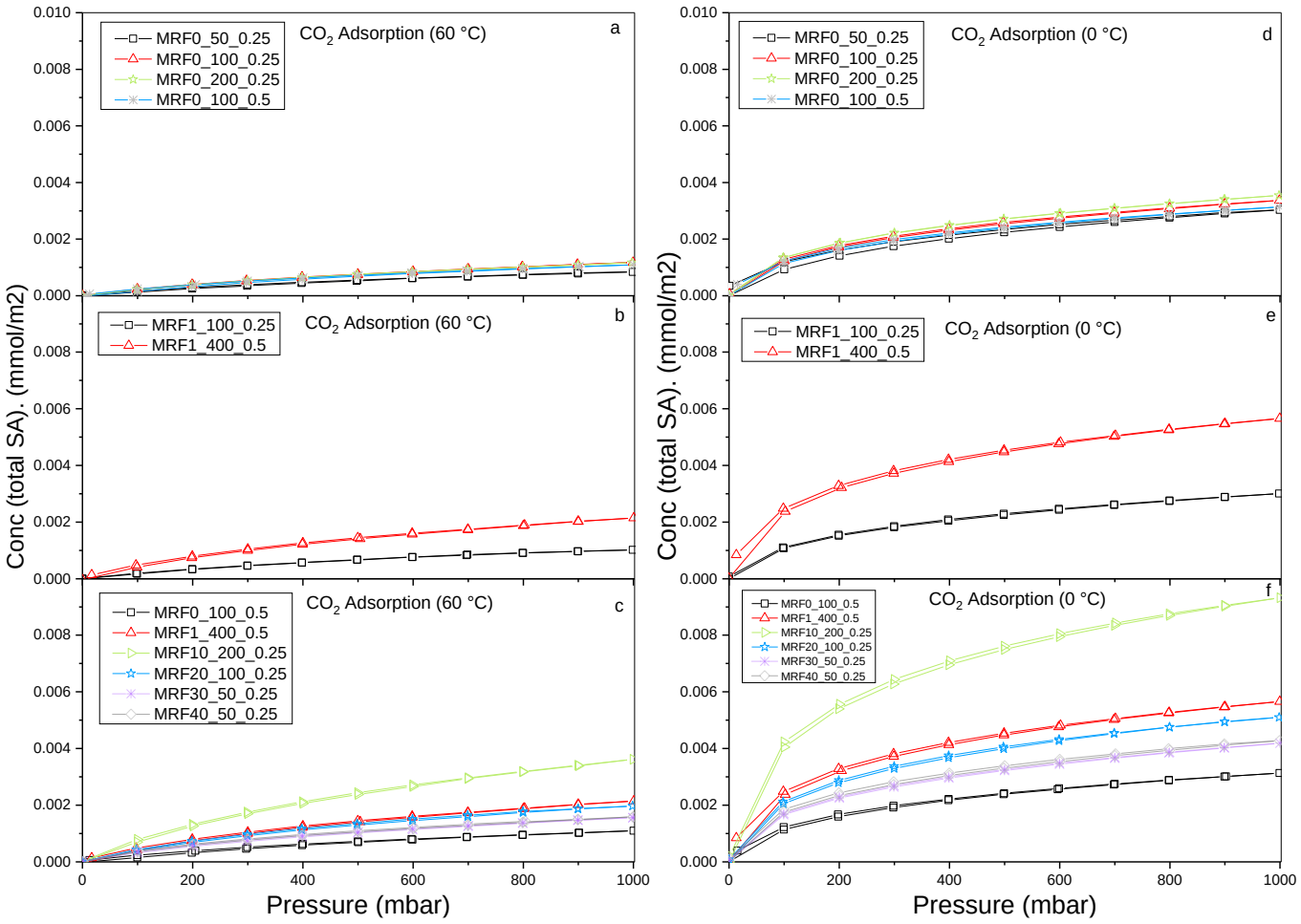

Figure 4: **CO_2 adsorption isotherm of MRF0_50_0.25, MRF0_100_0.25, MRF0_200_0.25 and MRF0_100_0.5 (a) at 60 °C and (d) at 0 °C. CO_2 adsorption isotherm of MRF1_100_0.25 and MRF1_400_0.5 (b) at 60 °C and (e) at 0 °C and CO_2 adsorption isotherm of MRF0_100_0.5, MRF1_400_0.5, MRF10_200_0.25, MRF20_100_0.25, MRF30_50_0.25 and MRF40_50_0.25 all samples of similar micropore volume (~0.03 cm^3/g) (c) at 60 °C and (f) at 0 °C.**

The isosteric enthalpies (ΔH_i) and entropies (ΔS_i) of adsorption were calculated at constant concentration of CO_2 adsorbed using Equation 2:

$$Ln(p) = \frac{\Delta H_i}{RT} - \frac{\Delta S_i}{R} \qquad Equation\ 2$$

where p is the pressure required to adsorb a given molar uptake of gas at temperature T, and R is the gas constant (8.314 J K^{-1} mol^{-1}). It is assumed that linearity is obeyed over the modest temperature range used.

The results obtained show a variation in enthalpy and entropy of adsorption of CO_2 on MRF xerogels with pressure for all materials studied. However, enthalpies of adsorption do not vary significantly with increasing [M]; with only ~1-2 kJ mol^{-1} difference for higher melamine contents compared to the MRF0 series (see Supporting Information Figure SI 11). In all cases, the heat of adsorption falls

within the range ~-30 to -25 kJ mol^{-1}, which is comparatively higher than the enthalpy of vaporization (15.3 kJ mol^{-1}) at -57.5 °C [35]. This indicates that adsorption is controlled by interactions other than condensation of the gas, likely enhanced adsorption effects by the microporous structures of these materials and, for the modified gels, further cooperative effects offered by the nitrogen centres incorporated from melamine. This suggests that the enthalpy of interaction between these two adsorption centres is comparable in strength. Entropies of adsorption decrease as concentration of adsorbed gas increases, indicating increasing order in the system, as expected in adsorption of gas species to a confined arrangement in the adsorbed phase, and the associated reduction in degrees of freedom. One drawback of amine scrubbing for carbon capture is the large regenerative energy penalty for amine recycling. Methylethylamine has been shown to exhibit heats of absorption in the range 60-80 kJ mol^{-1} of CO_2 at only 40 °C, and increased values at higher temperatures.[36] This suggests that adsorbing materials with enhanced amine interaction may provide a route to lower energy interactions than traditional amine scrubbing methods. Hence, it is advantageous to develop, not only materials with a good capacity for CO_2 but also, materials requiring lower thermal stimulus for gas recovery. The low energy penalty observed for CO_2 adsorption on the materials studied here suggests such a gain, with energies comparable with adsorption in microporous voids, potentially as a result of charge delocalisation effects on the melamine ring.

Kinetics can be determined from the real-time mass-time curves obtained for individual pressure steps obtained during measurements performed on the IGA system. CO_2 adsorption on porous MRF xerogels followed a stretched exponential (SE) mass transfer model in all cases, and kinetic parameters were determined over the whole pressure range studied (1 bar) at ~0 °C. The SE model is described by:

$$\frac{M_t}{M_e} = 1 - e^{-kt^{\beta_1}} \qquad \text{Equation 3}$$

where M_t and M_e are the mass uptake at time t and equilibrium, respectively, k is the rate constant and β is the exponent of adsorption. Previous work has demonstrated the applicability and validity of application of the SE model when evaluating adsorption dynamics [37-39]. The value of β indicates the dimensions involved in the adsorption process. Adsorption is 3-dimensional process when β = 1, and 1-dimensional when β = 0.5. β can also take intermediate values in the transition from 1- to 3-dimensionality. In an analogous definition to that given by Firestone *et al.* [40], who studied the microstructural relaxation of thin polymer films using the Kohlrausch-Williams-Watts (KWW 'stretched exponential') model, β, which reflects the relaxation times distribution, decreases with distribution broadening, demonstrating a wider range of relaxation times. β can also be equal to unity, removing the stretching factor on the exponent, representing a single relaxation time. Therefore, in terms of diffusional processes, β represents the distribution of relaxation times.

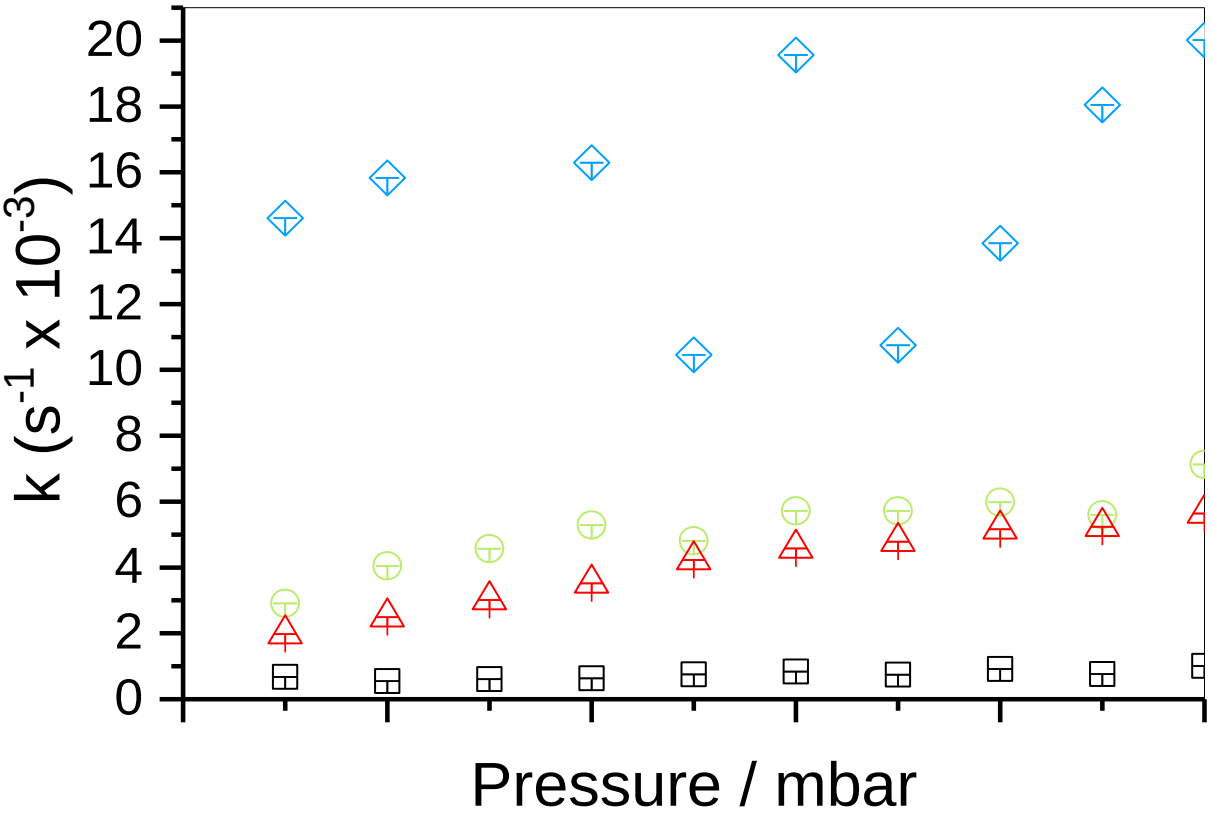

Figure 5: **Kinetic parameters obtained at 0 °C from the SE model: (a) rate constants (k) for adsorption of CO_2 on MRF xerogels: MRF0_50_0.25 (□), MRF0_100_0.25 (Δ), MRF0_100_0.5 (o) and MRF0_200_0.25 (◇).**

Figure 5 summarizes the rate constants obtained from the SE model to describe the kinetics of CO_2 adsorption onto MRF0 xerogels synthesised various R/C and R/F. Figure 5 shows that the kinetics of adsorption become faster as R/C is increased (see Supporting Information Figure SI 12-29) for modified gels. MRF0_100_0.5 shows similar behaviour as MRF0_100_0.25 suggesting that R/F has little effect on the kinetics of adsorption of CO_2 onto RF xerogels. There appears to be a trend in increasing rate of adsorption with increased R/C ratio, possibly as a consequence of widening of the pores within the material as the degree of crosslinking is reduced.

Adsorption on MRF xerogels involves diffusion through a porous network, parts of which may exhibit different shapes, such as bottle-neck-like or spherical; these differences markedly affect the diffusion of gas molecules through the material network. Physical adsorption of CO_2 onto the MRF xerogel surface should be enhanced by interactions between the adsorbate and surface functional groups; as [M] is increased, a higher number of interactions between CO_2 molecules and the MRF surface are expected. Rate constants obtained within this study also suggest that there is an increase in rate of adsorption, as well as strength of physical interaction; as [M] is increased from 0 through to 40 w/w%, the rate constants for adsorption demonstrate a small degree of variation around a plateau value of ~0.01 s^{-1} (Figure 6a). These values are more akin to the higher R/C ratio for unmodified materials, which may again be a consequence of the development of wider pores within the material increasing diffusional access up to a limiting value as stated. As pressure is increased (Figure 6b), the exponent tends to values closer to 1, suggesting a behaviour 'closer' to a Linear Driving Force model, which signifies a single relaxation time of adsorption, which may be related to

filling of smaller diameter pores and those remaining are of significantly large dimensions so as to pose no diffusional barrier to adsorption.

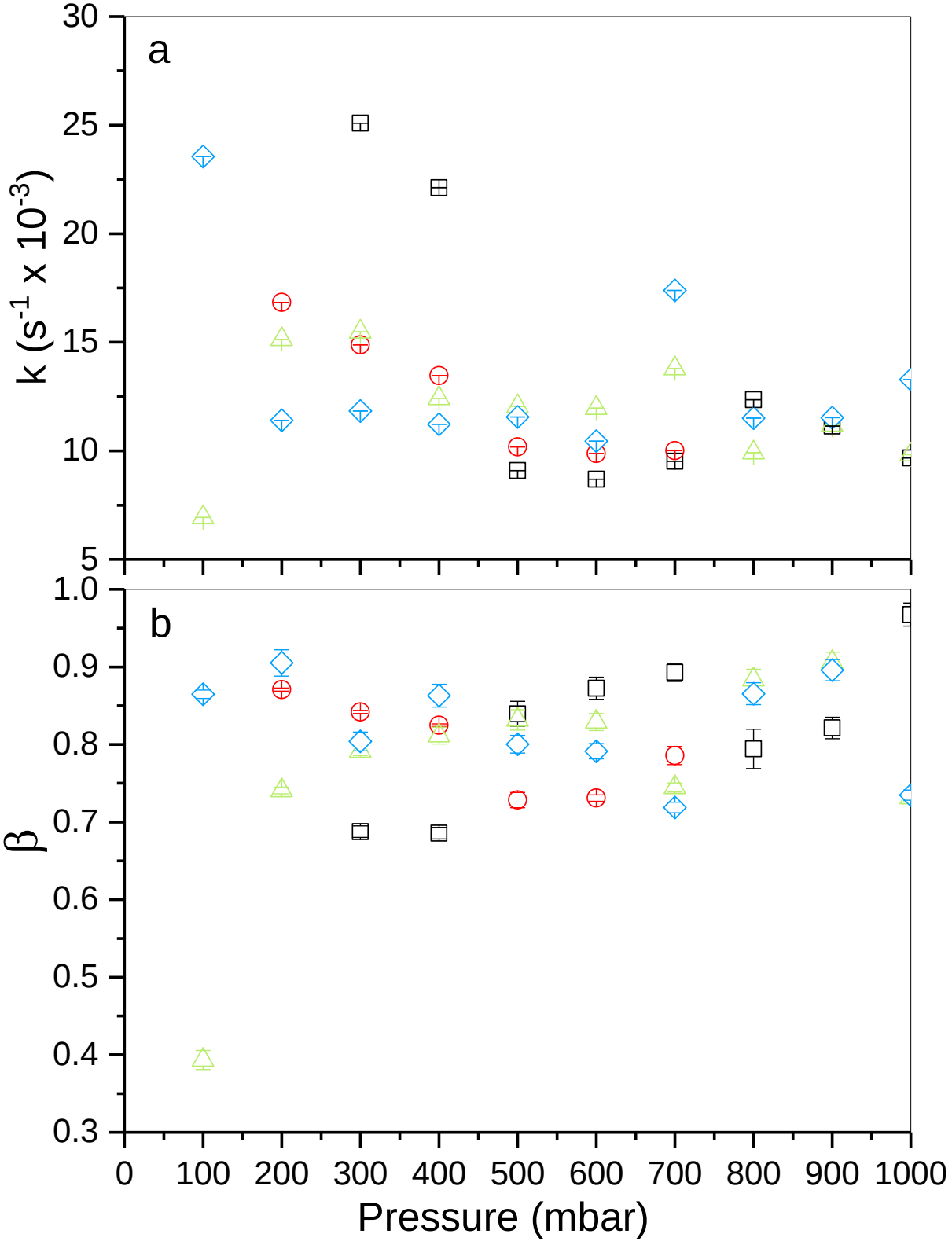

Figure 6: **Kinetic parameters obtained at 0 °C from the SE model: (a) rate constants (k) for adsorption of CO_2 on MRF xerogels and (b) the corresponding exponents (β): (□) MRF10_200_0.5, (o) MRF20_100_0.25, (Δ) MRF30_50_0.25 and (◇) MRF40_50_0.25.**

Physical adsorption is an exothermic process and uptake is enhanced at lower temperatures; however, due to the kinetic theory of gases, the rate of adsorption is increased at high temperatures, e.g. 60 °C, thus equilibrium is established more quickly and it is sometimes very difficult to assess the kinetics of adsorption. MRF0 xerogels exhibit rate constants for CO_2 adsorption of the same order of magnitude at both temperatures studied (Figure 5 and 7). By contrast, the exponent, β, exhibits higher values at higher temperature, suggesting behaviour more aligned with the LDF model at increased temperatures, i.e. a reduction in the width of the distribution or rate constants. It should also be noted that the β exponent tends to decrease as pressure is increased and a similar trend is observed for both temperatures. As R/C is increased, rate constant increases and the same observation is true for β. This trend is influenced by the increase in pore size, and pore volume, as R/C is increased, which facilitates diffusion of gases through the porous network of the gels. Again R/F has very little, or almost negligible, impact on the kinetics of adsorption of CO_2 on RF xerogels. MRF1_400_0.5 exhibits significantly higher rate constants at 60 °C than at 0 °C, in contrast, MRF1_100_0.25 exhibits rate constants of similar value at both temperatures, suggesting that the kinetics of gas diffusion through its structure are highly influenced by its narrow pore size distribution and more 'closed' structure in comparison to MRF1_400_0.5.

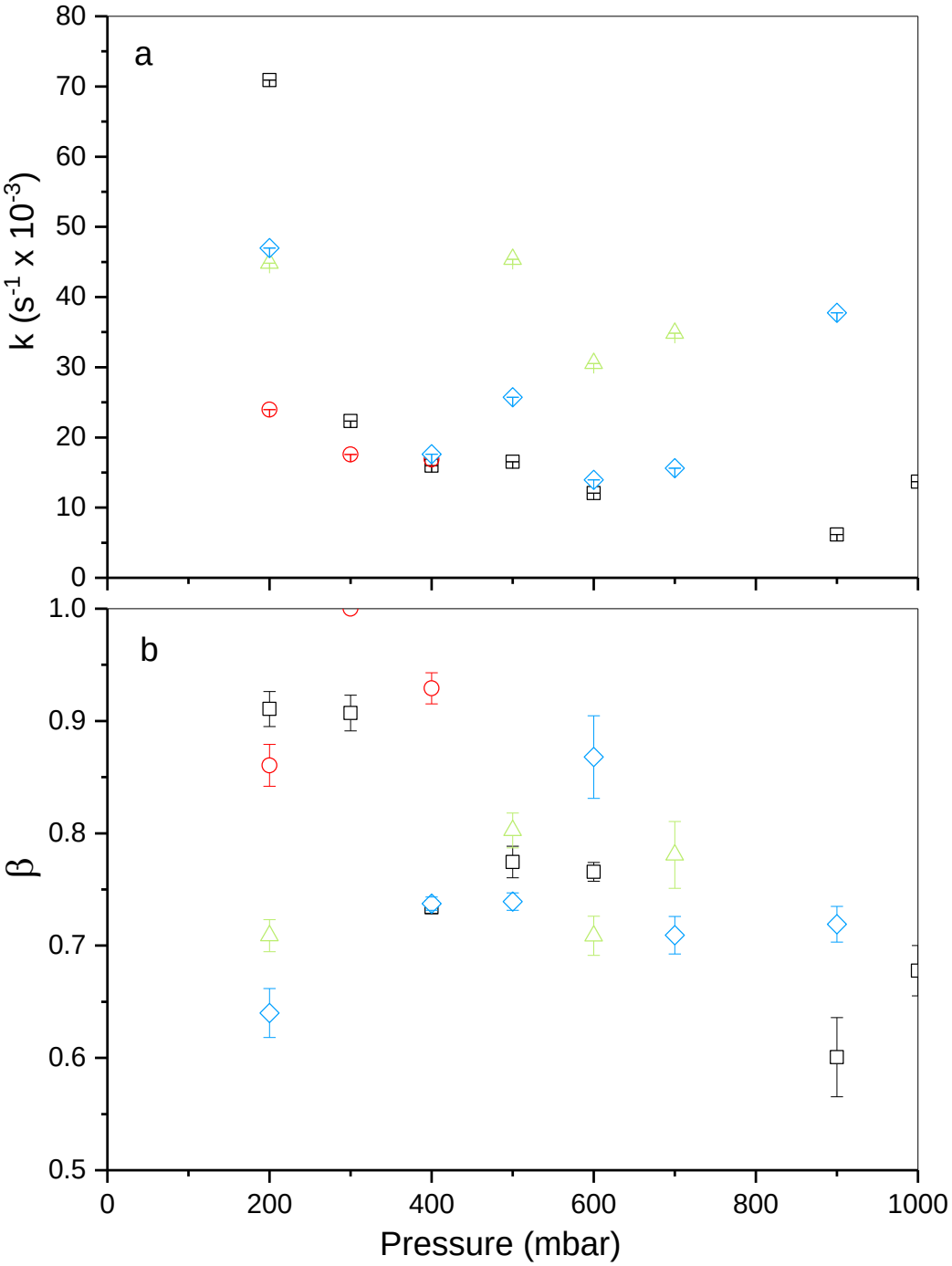

Figure 7: **Kinetic parameters obtained at 60 °C from the SE model: (a) rate constants (k) for adsorption of CO_2 on MRF xerogels and (b) the corresponding exponents (β), for (□) MRF10_200_0.5, (o) MRF20_100_0.25, (Δ) MRF30_50_0.25 and (◇) MRF40_50_0.25.**

The behaviour observed for higher melamine contents differs at 60 °C compared to 0 °C. The exponent tends to unity as pressure increases at 0 °C, while at 60 °C the opposite is true. Rate constants at 60 °C are significantly higher than those at 0 °C; however, at 0 °C they tend to decrease while at 60 °C they increase as pressure increases. Given the difficulty in obtaining rate constants at higher temperatures it was not possible to assess the full pressure range of (0-1000 mbar) in all cases.

Diffusional barriers to adsorption of CO_2 over the pressure range ~0-1000 mbar were calculated for pressure steps of ~100 mbar using the Arrhenius equation applied to the kinetic results obtained at 0 °C and 60 °C:

$$k = Ae^{-\frac{E_a}{RT}} \quad \text{Equation 4}$$

where *k* is the rate constant calculated from the SE kinetic model, *A* is the pre-exponential factor, *Ea* is the activation energy, *R* is the universal gas constant (8.314 J K^{-1} mol^{-1}) and *T* is the temperature of adsorption. The relationship between ln(A) and Ea (Figure 8) is in agreement with results reported for carbon based materials [37,41,42]. The data presented can be split into 3 subsets, the MRF0 series, MRF1 samples and higher [M] xerogels. As [M] increases, activation energies tend to higher values, suggesting an increase in the strength of the barriers to diffusion. There may be several contributions to an increase in diffusional barriers for these materials, such as charge effects, steric hindrance or CO_2 alignment onto adsorption sites; of these, there is, a more likely, and larger contribution from steric effects as a result of functional groups, such as amines from melamine, present on the surface. These groups might block, or partially block, the entrances of pores. Additionally, these groups would have thermal mobility; therefore, they would vibrate, especially at higher temperatures, which would result in potentially greater barriers at pore entrances. This contrasts, with the pore size increasing as [M] increases, which should minimize the aforementioned steric effect. However, as [M] is increased, pore volume and pore size also increase, while surface area decreases. Therefore, it can be assumed that the increase in pore volume does not necessarily result in an increase of 'useful' pore volume for CO_2 adsorption; however, these larger pores may be beneficial for mass transport within the structure. For instance, the average pore size is observed to increase from ~2 nm (MRF0_50_0.25) to ~12 nm (MRF10_200_0.25). For these larger pores, diffusion would not be affected by diffusional barriers, instead it can be considered as 'free diffusion'; therefore, the activation energy measured would be more likely related to diffusion through small pores present in these materials, i.e. pore diameters close to the molecular dimensions of the probe gas (3.189 Å x 3.339 Å x 5.361 Å) [43]. These small pores would suffer the same potential steric effects as their larger counterparts with increasing [M] and, therefore, an increase in activation energy would be observed.

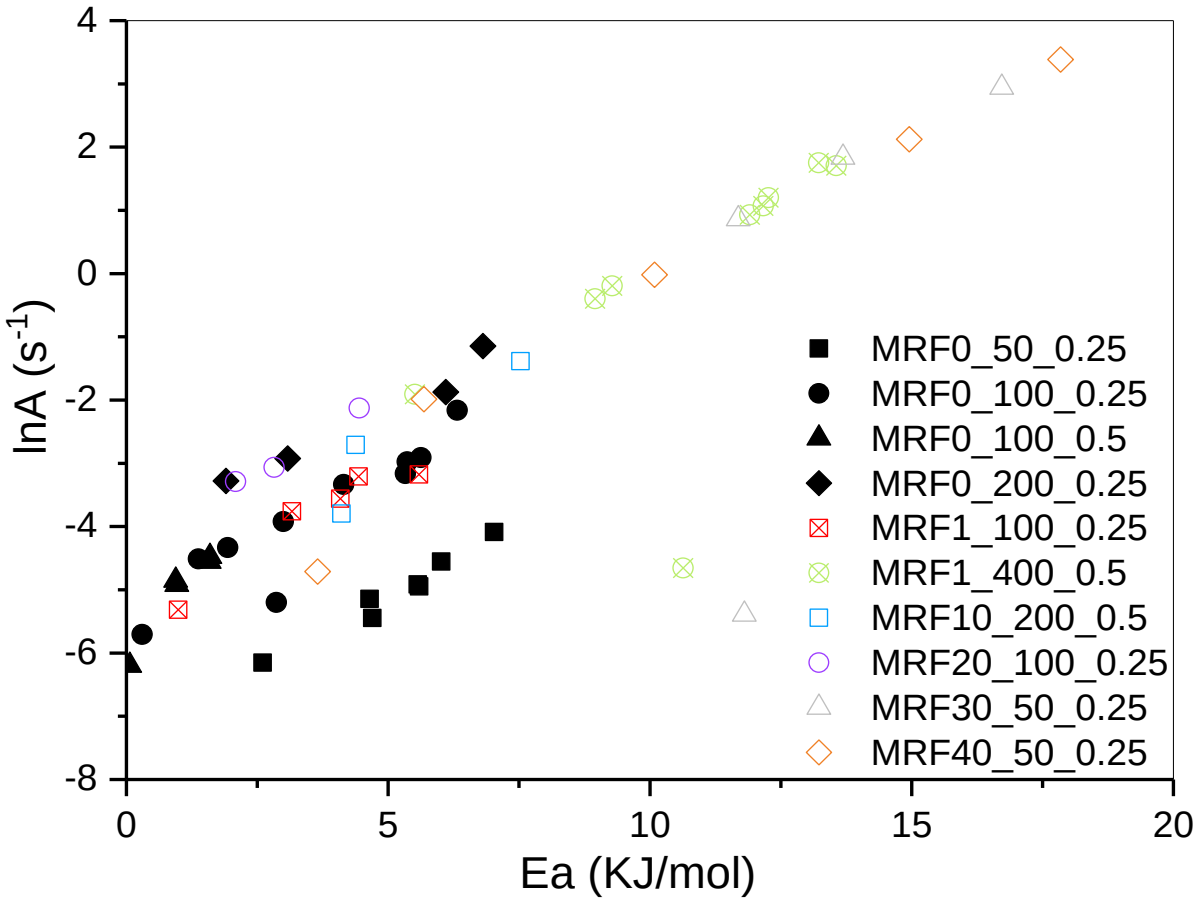

Figure 8: **Variation of ln (pre-exponential factor) (ln(A)) with activation energy (Ea) for adsorption of CO_2 on MRF xerogels.**

In addition to steric effects, alignment of CO_2 molecules onto specific adsorption sites may also affect kinetic energies. CO_2 molecules would interact differently with MRF0 (RF) than with a MRF xerogel synthesised with melamine, as a consequence of the chemical moieties present. While, CO_2 can adsorb on the graphitic basal planes of the gels, particularly in the micropores, there would be specific directionality onto the surface of a modified xerogel, when melamine is present, driven by the nitrogen group position. A CO_2 molecule would tend to be attracted to nitrogen, because of its free lone pair of electrons, which interact with the partial positive charge on the carbon of CO_2, induced as a result of the electronegativity of the bonded oxygen atoms. As a consequence, the carbon atom would need to align with the nitrogen, which suggests that not all collisions would be successful, hence, the rate of adsorption would be affected. Given the pore volumes determined for the ten materials tested in this study, it can be seen that the CO_2 uptakes at 0 °C exceed the micropore volume in all cases, potentially as a result of enhanced interactions with the material surface i.e. nitrogen functionalities. This accounts for the increase in uptake as [M] increases; the activation energies observed here, in conjunction with the low energy penalty (heat of adsorption within the range ~-30 to -25 kJ mol^{-1}, see Figure SI 11) observed for those MRF of higher melamine content, suggests that CO_2 adsorption on MRF xerogels would be kinetically rather than thermodynamically controlled.

A series of CO_2 adsorption-desorption cycling tests were performed to assess the long-term working capacities, and stabilities, of the 10 samples studied in this chapter. Most samples underwent 90

cycles (charge and discharge) and one sample (MRF1_100_0.25) was exposed to 500 cycles. Results of these cycling studies show that MRF xerogels have the ability to retain their reversible storage capacity over the cycle interval tested, suggesting long term stability in terms of uptake and the samples themselves. This is complementary to the thermal stability results obtained by thermo-gravimetric analysis. Adsorption capacity can be measured as the difference between the charge and discharge cycles (Figure 10).

There is a significant increase in adsorption capacity for samples MRF0_50_0.25, MRF0_100_0.25 and MRF0_200_0.25 (see Supporting Information Figure SI 30). This enhanced capacity can be directly linked with the increase in R/C. As R/C increases so too do pore size and pore volume (Table 1), producing adsorption capacity that can be accessed more easily for the larger pore sizes. MRF0_100_0.5 exhibits an adsorption capacity slightly larger than MRF0_100_0.25, suggesting that, contrastingly, R/F has no significant impact on capacity, in line with the textural characteristics observed.

MRF1_400_0.5 shows an enhanced adsorption capacity compared to MRF1_100_0.25 (see Supporting Information Figure SI 31), which, as previously observed, can be attributed to the larger value of R/C used. It is important to note that the adsorption capacity of MRF1_400_0.5 has been observed to be stable up to 1000 cycles, suggesting the high regenerative ability of this material.

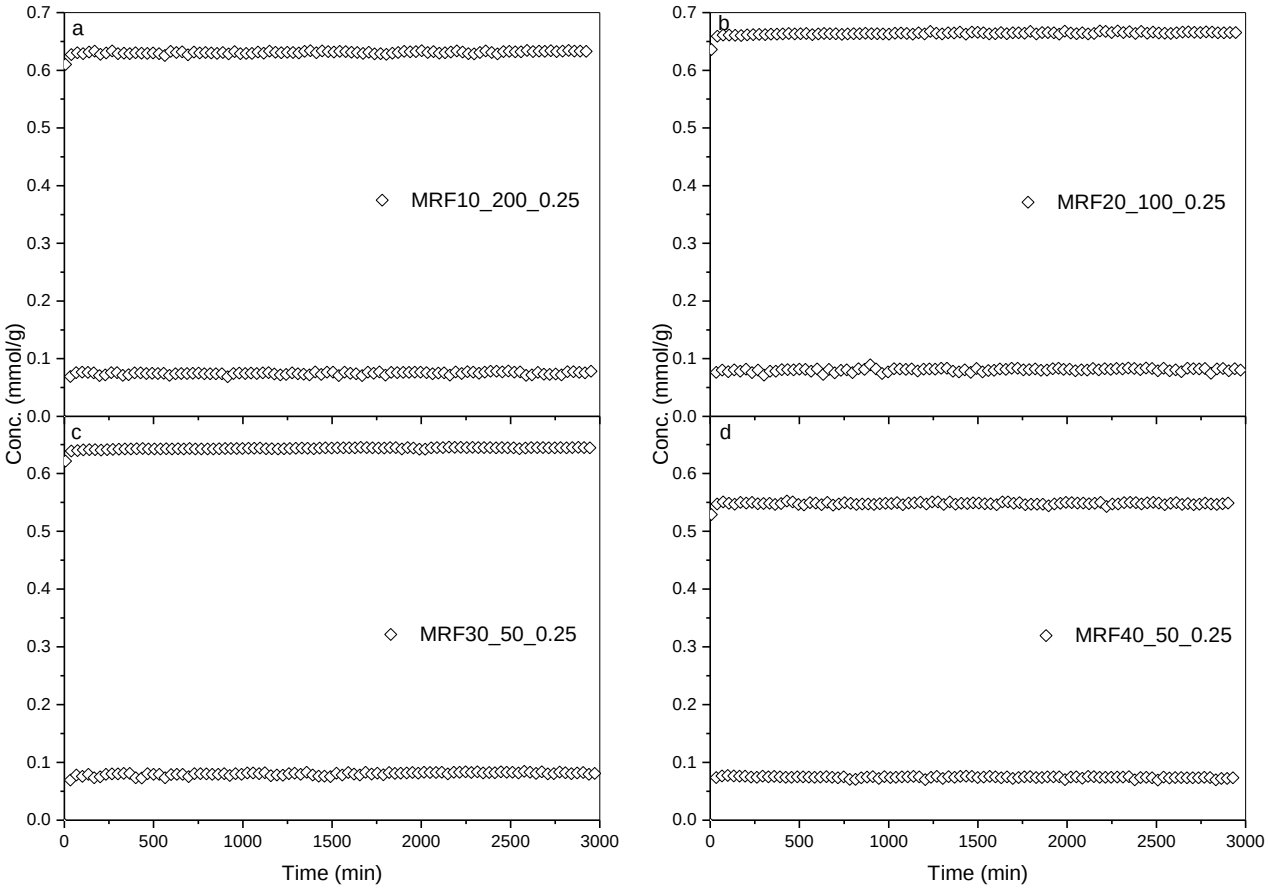

Figure 9: **CO_2 adsorption capacities for cycling adsorption experiments (Pmin = 50 mbar, Pmax = 1000 mbar; T = 60 °C): (a) MRF10_200_0.25 over 90 cycles; (b) MRF20_100_0.25 over 90 cycles; (c) MRF30_50_0.25 over 90 cycles and (d) MRF40_50_0.5 over 90 cycles. Maxima and Minima values only shown for clarity.**

The reversible quantity of CO_2 adsorbed, at a given temperature, between the lower and upper operating pressures of a system (Figure 10), is more industrially important than the single maximum adsorption capacity. Adsorption isotherm shape defines the pressure range in which most of the reversible uptake occurs, however, the rate of adsorption/desorption will affect this property due to kinetic limitations. The shapes of the adsorption isotherms obtained for CO_2 on the MRF xerogels studied here were Type I (microporous), therefore, the storage adsorption capacity will be defined by the lowest range of pressure selected. The amount of CO_2 adsorbed per unit mass of material defines the gravimetric storage capacity (Figure 10), which clearly increases as [M] is increased, with a maximum observed for MRF20_100_0.25, after which storage capacity falls despite the increase in [M]. This final reduction is likely due to the proportion of melamine in the synthetic matrix impinging on the ability of the gel network to successfully crosslink, producing a weaker gel, which may impact on accessibility of nitrogen functionalities within the material.

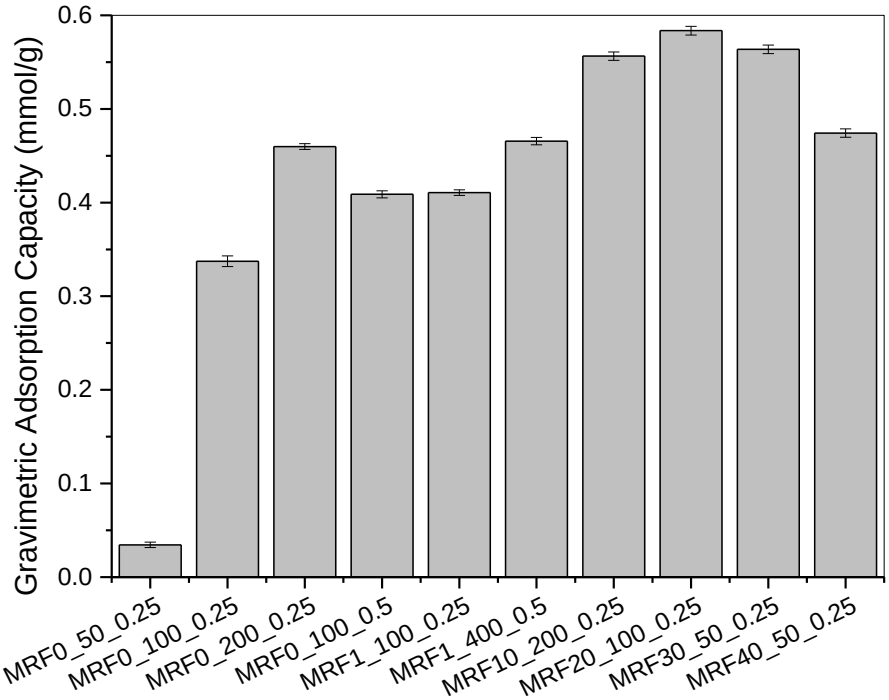

Figure 10: Gravimetric adsorption capacities of MRF xerogels of variable R/C, R/F and [M], as determined from cycling adsorption experiments (Pmin = 50 mbar, Pmax = 1000 mbar; T = 60 °C)

Conclusions

Ten materials were selected from a suite of 100 samples produced previously in a parametric study of resorcinol-formaldehyde gel synthesis [25], with incremental substitution of resorcinol by melamine. The results obtained for the initial suite of materials showed that increasing [M] results in a linear increase in nitrogen content, with enhanced presence of imide functionalities. Most notably in this work, increasing [M] had a similar effect to increasing R/C, i.e. reduced surface area and pore volume, with increased pore size.[25] Samples were chosen on the basis of their micropore volume and varying N content. 6 samples had very similar micropore volume with different levels of nitrogen content (0, 1, 10, 20, 30 and 40), while 3 MRF0 samples with increasing R/C (50, 100 and 200) and 1 additional MRF1 sample with high R/C (400) were also chosen. The 10 selected samples were analysed and characterised for CO_2 adsorption, and allowed evaluation of increasing resorcinol:catalyst ratio, increasing melamine concentration and comparison between resorcinol:formaldehyde ratio (0.25 and 0.5). An increase in carbon basic surface functionalities was observed as melamine concentration was increased, which agrees with the reduction of acidic contributions from phenolic groups, as melamine concentration increases. C=O bonding was found to increase as melamine concentration increases, which is attributed to polymerization reactions. Thermal stability showed a similar trend, with an increase in volatile matter as melamine concentration increased, while fixed carbon decreased; this dichotomy accounts for the mechanical weaknesses observed as melamine concentration increases, the result of weaker crosslinking.

CO_2 adsorption capacities, measured at 0 and 60 °C, show a decrease with increasing temperature; however, CO_2 adsorption capacity increases, at both temperatures, as melamine concentration increases, with a maximum at 20 w/w% melamine. Heat of adsorption does not vary significantly with increasing melamine concentration (~-30 to -25 kJ mol^{-1}) and, as expected, entropy decreases as the amount adsorbed increases, due to ordering of the adsorptive. The low enthalpy of adsorption suggests that MRF xerogels would be easy to regenerate, particularly compared to liquid amine sorbents. Kinetics of adsorption, at both temperatures, were described by a stretched exponential model, with increasing rate of adsorption as [M] increases. As R/C increases, so too does pore size, which facilitates gas diffusion through the network of MRF xerogels, hence, adsorption rate increases with resorcinol:catalyst ratio. Generally, rate of adsorption increases as melamine concentration increases, and with temperature. Activation energies were generally low (0-20 kJ/mol) and increase with increasing melamine concentration, suggesting increased barriers to diffusion, by either steric, chemical or alignment effects. CO_2 regeneration ability was tested by pressure swing cycling; in all cases, adsorption capacity increased as melamine concentration increased and the long-term stability observed suggest that optimised xerogels modified by nitrogen-rich precursors could present alternatives for future carbon capture systems.

Acknowledgements

Thanks to the Department of Chemical and Process Engineering and the University of Strathclyde for their support. Authors also want to thank NEXUS, National EPSRC XPS facilities of Newcastle University.

References

1. Lippens, B. C., and De Boer, J., *Journal of Catalysis* (1965) **4** (3), 319
2. Thommes, M.*, et al.*, *Pure and Applied Chemistry* (2015) **87** (9-10), 1051
3. Wilcox, J.*, et al.*, *Annual Review of Chemical and Biomolecular Engineering* (2014) **5** (1), 479
4. Adewole, J. K.*, et al.*, *International Journal of Greenhouse Gas Control* (2013) **17** (0), 46
5. Scholes, C. A.*, et al.*, *International Journal of Greenhouse Gas Control* (2010) **4** (5), 739
6. Olajire, A. A., *Energy* (2010) **35** (6), 2610
7. Ma, Z. W.*, et al.*, *Renewable and Sustainable Energy Reviews* (2016) **53**, 1273
8. Xu, C.-G., and Li, X.-S., *RSC Advances* (2014) **4** (35), 18301
9. Li, Z.*, et al.*, *Journal of Natural Gas Science and Engineering*
10. Ebrahimi, A.*, et al.*, *Energy* (2015) **90, Part 2**, 1298
11. Burt, S. B., Andrew; Baxter, Larry, *Sustainable Energy Solutions; Brigham Young University*
12. Fu, D.*, et al.*, *Energy* (2016) **113**, 1
13. Fu, D.*, et al.*, *The Journal of Chemical Thermodynamics* (2016) **101**, 123
14. Nwaoha, C.*, et al.*, *Journal of Natural Gas Science and Engineering* (2016) **33**, 742
15. Yu, C.-H.*, et al.*, *Aerosol and Air Quality Research* (2012) **12** (5), 745
16. Rochelle, G. T., *Current Opinion in Chemical Engineering* (2012) **1** (2), 183
17. Wang, J.*, et al.*, *Energy & Environmental Science* (2014) **7** (11), 3478
18. Samanta, A.*, et al.*, *Industrial & Engineering Chemistry Research* (2012) **51** (4), 1438
19. Choi, S.*, et al.*, *ChemSusChem* (2009) **2** (9), 796
20. Gray, M. L. S., Y.; Champagne, K. J.; Pennline, H.; Stevens, R. W. Jr.; Toochinda, P.; Chuang, S.S.C., *Div. Fuel Chem., Am. Chem Soc. - Prepr. Symp.* (2002) **47**, 63
21. Razavi, S. S.*, et al.*, *Journal of molecular modeling* (2011) **17** (5), 1163
22. Guo, B.*, et al.*, *Journal of Natural Gas Chemistry* (2006) **15** (3), 223
23. Mirzaeian, M., and Hall, P. J., *Journal of materials science* (2009) **44** (10), 2705
24. Chen, J. P., and Wu, S., *Langmuir* (2004) **20** (6), 2233
25. Principe, I. A., and Fletcher, A. J., *Materials Today Chemistry* (2018) **7**, 5
26. Pekala, R. W., *Journal of Materials Science* (1989) **24** (9), 3221

27. Brunauer, S.*, et al.*, *Journal of the American Chemical Society* (1938) **60**, 309
28. Rouquerol, J.*, et al.*, Is the BET equation applicable to microporous adsorbents? In *Studies in Surface Science and Catalysis*, P.L. Llewellyn, F. R.-R. J. R., and Seaton, N., (eds.) Elsevier(2007), Vol. Volume 160, pp 49
29. Barrett, E. P.*, et al.*, *Journal of the American Chemical Society* (1951) **73**, 373
30. Gebert, M. S., and Pekala, R. W., *Chemistry of Materials* (1994) **6** (2), 220
31. Yamamoto, T.*, et al.*, *Journal of Non-Crystalline Solids* (2001) **288** (1–3), 46
32. Williams, D. H., and Fleming, I., *Spectroscopic methods in organic chemistry*. Fourth edition ed.; McGraw-Hill: 1980
33. Pels, J.*, et al.*, *Carbon* (1995) **33** (11), 1641
34. Ullah, S.*, et al.*, *The Scientific World Journal* (2014) **2014**
35. Center, Q. d. C. E. R. I., Pure components properties.
36. Kim, I., and Svendsen, H. F., *Industrial & engineering chemistry research* (2007) **46** (17), 5803
37. Fletcher, A. J., and Thomas, K. M., *Langmuir* (2000) **16** (15), 6253
38. Fletcher, A. J., and Thomas, K. M., *The Journal of Physical Chemistry C* (2007) **111** (5), 2107
39. Fletcher, A. J.*, et al.*, *The Journal of Physical Chemistry C* (2007) **111** (23), 8349
40. Firestone, M. A.*, et al.*, *Macromolecules* (1995) **28** (7), 2260
41. Reid, C., and Thomas, K., *Langmuir* (1999) **15** (9), 3206
42. Reid, C.*, et al.*, *Langmuir* (1998) **14** (9), 2415
43. Webster, C. E.*, et al.*, *Journal of the American Chemical Society* (1998) **120** (22), 5509